Acta Oceanol. Sin., 2021, Vol. 40, No. 11, P. 1–10
https://doi.org/10.1007/s13131-021-1743-0
http://www.aosocean.com
E-mail: ocean2@hyxb.org.cn

Estimate of contribution of near-inertial waves to the velocity shear in the Bay of Bengal based on mooring observations from 2013 to 2014

Shanwu Zhang[1], Yun Qiu[1, 2, 3], Hangyu Chen[1], Junqiang Shen[1], Junpeng Zhang[1], Jing Cha[1], Fuwen Qiu[1], Chunsheng Jing[1]*

[1] Third Institute of Oceanography, Ministry of Natural Resources, Xiamen 361005, China

[2] Laboratory for Regional Oceanography and Numerical Modeling, Pilot National Laboratory for Marine Science and Technology (Qingdao), Qingdao 266237, China

[3] Southern Marine Science and Engineering Guangdong Laboratory (Zhuhai), Zhuhai 519082, China

Received 15 August 2020; accepted 12 September 2020

Abstract

Near-inertial motions contribute most of the velocity shear in the upper ocean. In the Bay of Bengal (BoB), the annual-mean energy flux from the wind to near-inertial motions in the mixed layer in 2013 is dominated by tropical cyclone (TC) processes. However, due to the lack of long-term observations of velocity profiles, our knowledge about interior near-inertial waves (NIWs) as well as their shear features is limited. In this study, we quantified the contribution of NIWs to shear by integrating the wavenumber-frequency spectra estimated from velocity profiles in the upper layers (40–440 m) of the southern BoB from April 2013 to May 2014. It is shown that the annual-mean proportion of near-inertial shear out of the total is approximately 50%, and the high contribution is mainly due to the enhancement of the TC processes during which the near-inertial shear accounts for nearly 80% of the total. In the steady monsoon seasons, the near-inertial shear is dominant to or at least comparable with the subinertial shear. The contribution of NIWs to the total shear is lower during the summer monsoon than during the winter monsoon owing to more active mesoscale eddies and higher subinertial shear during the summer monsoon. The Doppler shifting of the M_2 internal tide has little effect on the main results since the proportion of shear from the tidal motions is much lower than that from the near-inertial and subinertial motions.

Key words: near-inertial waves, shear, monsoon, tropical cyclone, Bay of Bengal

Citation: Zhang Shanwu, Qiu Yun, Chen Hangyu, Shen Junqiang, Zhang Junpeng, Cha Jing, Qiu Fuwen, Jing Chunsheng. 2021. Estimate of contribution of near-inertial waves to the velocity shear in the Bay of Bengal based on mooring observations from 2013 to 2014. Acta Oceanologica Sinica, 40(11): 1–10, doi: 10.1007/s13131-021-1743-0

1 Introduction

The vertical shear of horizontal currents (hereinafter referred to as velocity shear or shear) induced by near-inertial waves (NIWs), in contrast with that caused by internal tides, which mostly originate from ocean bottom through interaction of the barotropic tide and bottom topography, is more prominent in the upper ocean and is typically dominant over the total shear (Garrett, 2001; Alford et al., 2016). Characterization of the sources, scales and variability of ocean shear is an important goal of physical oceanography since shear instability is a major contributor to driving turbulence in the open ocean thermocline (Alford et al., 2017). Previous work has reported that 70% of the total shear variance for a short (14 d) record of depth-time series in the Banda Sea is attributed to downward propagating NIWs (Alford and Gregg, 2001). A recent contribution based on six moorings existing for 5 to 9 months in the northern South China Sea has shown that shear caused by NIWs is approximately 20%–25% of the total, although NIWs only account for 2%–7% of the total current variance (Cao et al., 2019). Thus, the contribution of NIWs to shear may vary depending on the duration and location of the observation, and it is necessary to quantify the value and show its variability for a specified basin.

The Bay of Bengal (BoB) is a tropical basin characterized by reversing monsoons (Varkey et al., 1996; Schott et al., 2009). NIWs in the BoB can be generated by changing wind magnitude rather than the inertial rotation of wind forces (Majumder et al., 2015; Johnston et al., 2016). It is also a region affected by abundant tropical cyclones (TCs), which are particularly efficient generators for NIWs (Girishkumar et al., 2014). During 2013, the BoB suffered from several TCs. Unlike the work done by surface winds on the near-inertial motions that is generally high in the southeast of Sri Lanka (Fig. S1), the annual-mean near-inertial energy flux into the mixed layer is enhanced along the paths and mostly on the right side of the TCs (Fig. 1). The maximum flux appears in

Foundation item: The National Key Research and Development Program of China under contract No. 2016YFC1401403; the State Oceanic Administration (SOA) Program on Global Change and Air-Sea Interactions under contract No. GASI-IPOVAI-02; the China Ocean Mineral Resources R & D Association under contract No. DY135-E2-4; the Scientific Research Foundation of Third Institute of Oceanography, SOA under contract Nos 2018001, 2017012 and 2014028.
*Corresponding author, E-mail: jingcs@tio.org.cn

the northern BoB where TC Phailin reaches its peak strength. The value is approximately 80 mW/m², dozens of times higher than the climatological value, which is estimated to be 2.4 mW/m² for the basin average. Moreover, the basin-averaged flux for 2013 is significantly higher (3.7 mW/m²) due to the much higher near-inertial energy input from the TCs. Basically, the annual-mean flux in the BoB is comparable with that in the mid-latitude storm track region (Alford, 2003; Johnston et al., 2016).

On the other hand, cold surface biases are common in most coupled models of the BoB, which may be attributed to the inadequate parametrization of vertical mixing (Chowdary et al., 2016; Goswami et al., 2016). Among those mixing-related and unresolved processes in the coupled models, NIWs can be a key candidate owing to their high contribution to the upper ocean shear (Jochum et al., 2013). A previous study reported that the near-inertial oscillations in the thermocline of the BoB during the relaxation stage of TC Jal in 2010 allow much freer turbulent exchange between the mixed layer and thermocline, contributing the majority of the mixed layer heat budget (Girishkumar et al., 2014). A more recent study by Cherian et al. (2020) found that strong mixing events during monsoon seasons occur concurrently with enhanced shear from downward-propagating NIWs and other low-frequency monsoon currents and mesoscale features. The vertical mixing associated with these high shear processes contributes to the turbulent transport of salt, of which the magnitude can approximately close the model-based salt budgets for the upper BoB.

The high near-inertial energy input from the monsoon and TCs and the high shear nature of NIWs shows the need for characterization of the shear features of NIWs in the BoB. However, due to limited long-term measurements of velocity profiles, it remains unclear to what extent NIWs contribute to the total shear and therefore to the vertical mixing in the upper BoB. In this study, using velocity measurements from a subsurface mooring in the BoB (Fig. 1), we quantified the contribution of NIWs to shear in the upper ocean interior, and discuss the role of NIWs in the vertical mixing of this monsoon-driven basin.

The rest of the article is arranged as follows. The mooring data and processing methodology are presented in Section 2. In Section 3, we show the main results based on the velocity data analysis. A brief discussion is given in Section 4. A summary and conclusions are presented in Section 5.

2 Materials and methods

2.1 *Data*

The data were from a subsurface mooring deployed in the water of 3 428 m near 10°N, 88°E. The velocity data were obtained from a Teledyne 75 kHz Acoustic Doppler Current Profile (ADCP) functioning from April 9, 2013 to May 11, 2014. The ADCP was mounted at a depth of approximately 470 m and measured the current profiles from 40 m to approximately 440 m each hour in 16 m bins, and the shear was computed by first differencing the velocity over each bin. There was a conductivity temperature depth (CTD) chain above the ADCP that consisted of fifteen temperature loggers, two temperature and conductivity sensors and two CTD sensors spanning from 270 m to 450 m that were separated by 10 m intervals. The CTD chain returned averaged temperature data every 10–30 min, and during postprocessing, the data were rearranged into 1 h intervals to match the velocity data. The temperature data are used since they indicate signals of mesoscale eddies and can be used to characterize the eddy features together with the sea surface anomaly (SLA) data.

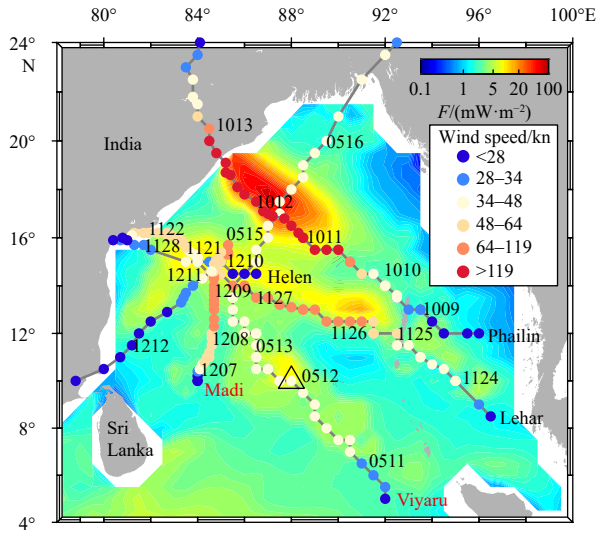

Fig. 1. Distribution of annual-mean near-inertial energy flux (colors) in the BoB in 2013. The mooring location is indicated by the black triangle. Gray solid lines and color dots give the paths and strength levels of TCs in 2013, respectively. Dates (MMDD) are marked along the tracks besides the dots. The color dots represent the maximum sustained wind speed (in knots) of the TCs. The near-inertial energy flux (F) is computed by solving the Pollard-Millard slab model using the spectral method (Alford, 2003) with National Centers for Environmental Prediction (NCEP) Climate Forecast Version 2 (CSFv2) 6-hourly wind data (Saha et al., 2014) with the mixed layer depth in the slab model set to 15 m.

The observed meridional velocity and shear are presented in Fig. 2, as are the NCEP wind vectors, which clearly show seasonal reversal of the monsoons. The whole record is divided into six forcing periods according to the season partition for the BoB given in Varkey et al. (1996), with two additional TC processes (Viyaru and Madi) in 2013. Also depicted are the vertical mean of the horizontal kinetic energy (KE),

$$\mathrm{KE} = \frac{1}{2}\rho_0 \left(u^2 + v^2\right), \tag{1}$$

and the magnitude of the shear,

$$|S| = \sqrt{u_z^2 + v_z^2}, \tag{2}$$

for the upper 40–440 m. Here, ρ_0 is the density, u and v are the east and north components of the velocity, and u_z and v_z are the vertical shear of u and v, respectively. Both the total and band-pass filtered near-inertial KE and shear magnitude are shown, where the near-inertial band is simply defined as between 0.75 and 1.25 of the local Coriolis frequency, f (about 0.35 cpd (cycle per day) at 10°N). The observed velocity and shear show apparent near-inertial wakes following changes in surface winds, especially during TC processes (Figs 2b and d). Note that the near-inertial KE is far lower than the total KE, while the near-inertial shear is comparable with the total shear and may dominate during TC processes (Figs 2c and e).

2.2 *Data analysis*

Prior to spectral analysis, the shear data were first Wentzel–Kramers–Brillouin (WKB) scaled to minimize the refraction of

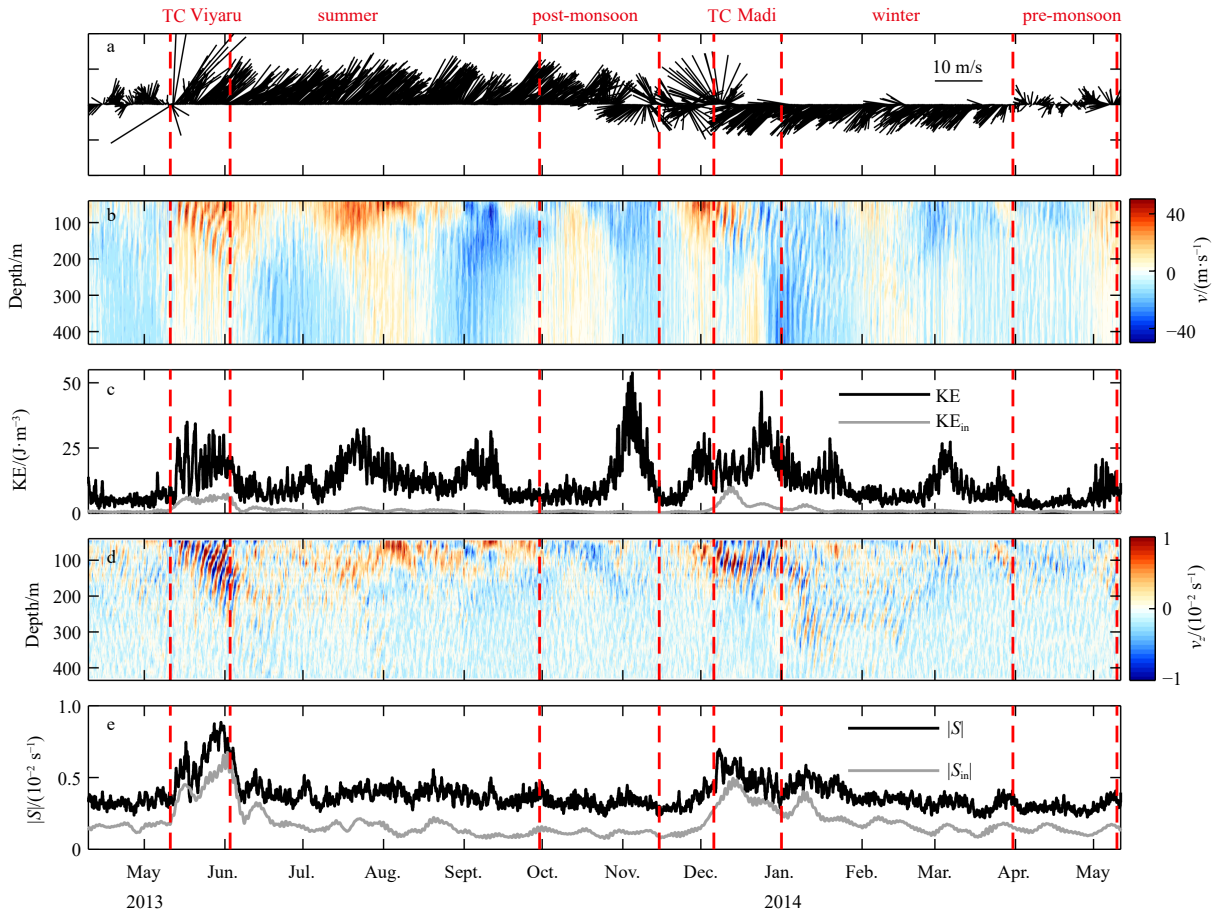

Fig. 2. Mooring observations of the velocity and shear. Surface wind acquired from the NCEP CFSv2 6-hourly winds (a), observed meridional velocity (b), vertical mean of the total and near-inertial KE (c), vertical gradient of the meridional velocity (d), and vertical mean of the magnitude of the total shear and near-inertial shear (e). The red dashed lines divide the observations into six periods: TC Viyaru (May 11–June 3, 2013), summer monsoon (June–September, 2013), post-monsoon (October–mid November, 2013), TC Madi (December 6–31, 2013), winter monsoon (January–March, 2014) and pre-monsoon (April 1–May 11, 2014).

NIWs propagating in variable stratification (Leaman and Sanford, 1975). The shear data were multiplied by the following factor: $[N(z)/<N>]^{1/2}$, where N is the buoyancy frequency derived from the climatological profile of World Ocean Atlas 2018 (WOA 2018) at the mooring site and $<N>$ = 5.62 cph (cycle per hour) is the depth-mean of N between 40 m and 440 m (Figs 3a and b). Accordingly, the vertical depth was WKB-stretched (Fig. 3c). The stretched depth was computed as follows:

$$z' = \int_{40}^{z} \frac{N}{< N >} \mathrm{d}z. \tag{3}$$

Straighter phase lines in the WKB-stretched depth would indicate the applicability of the WKB-scaled method.

The following semiempirical plane-wave fit method (Alford and Gregg, 2001) was used to extract the observed frequency and vertical wavenumber fora specified NIW event:

$$\Psi = \mathrm{Re}\{\hat{\Psi}(z) \exp[2\pi \mathrm{i}(\omega_0 t - m_0 z' + \phi_\Psi)]\}, \tag{4}$$

where ω_0 and m_0 are the frequency and wavenumber, and $\widehat{\Psi}(z)$ and ϕ_Ψ are the amplitude and phase, respectively. For each NIW event, the parameters (m_0 and ω_0) were chosen to maximize the variance explained by the plane wave solution, and the group velocity was estimated from the downward migration of near-inertial energy.

The NIW events were identified as slanted phase lines with elevated shear. This was achieved by applying a vector correlation between the total shear and the bandpass filtered near-inertial shear (Fig. 4a) at each depth. The vector correlation method gives the coordinate-independent linear correlation between two vectors (Breaker et al., 2003). The correlation coefficient ranges from 0 (no correlation) to $\sqrt{2}$ (perfect correlation). A value of 0.7 was chosen to separate the elevated shear events from the weak ones (Fig. 4b). Two events during the TC processes were selected as examples. The plane wave solutions explain 72% and 76% of the variance for event 1 (TC Viyaru) and event 2 (TC Madi), respectively, giving good approximations to the NIW events (Figs 4c and d). The corresponding observed frequencies fitted are 0.88f and 0.95f, both of which suggested lower shifts in the effective inertial frequency by background vorticity. The vertical wavenumbers fitted are 0.007 cpm (cycle per meter) (λ_z = 143 m) and 0.005 cpm (λ_z = 200 m), respectively. Moreover, the snapshots of the straight phase lines in Figs 4c and d suggested the applicability of the WKB scale and motivated further analysis on the shear data.

Two-dimensional Fourier transforms, $\widetilde{w}(\omega, m)$ were applied to the WKB-scaled shear, u_z+iv_z and multiplied by Hanning win-

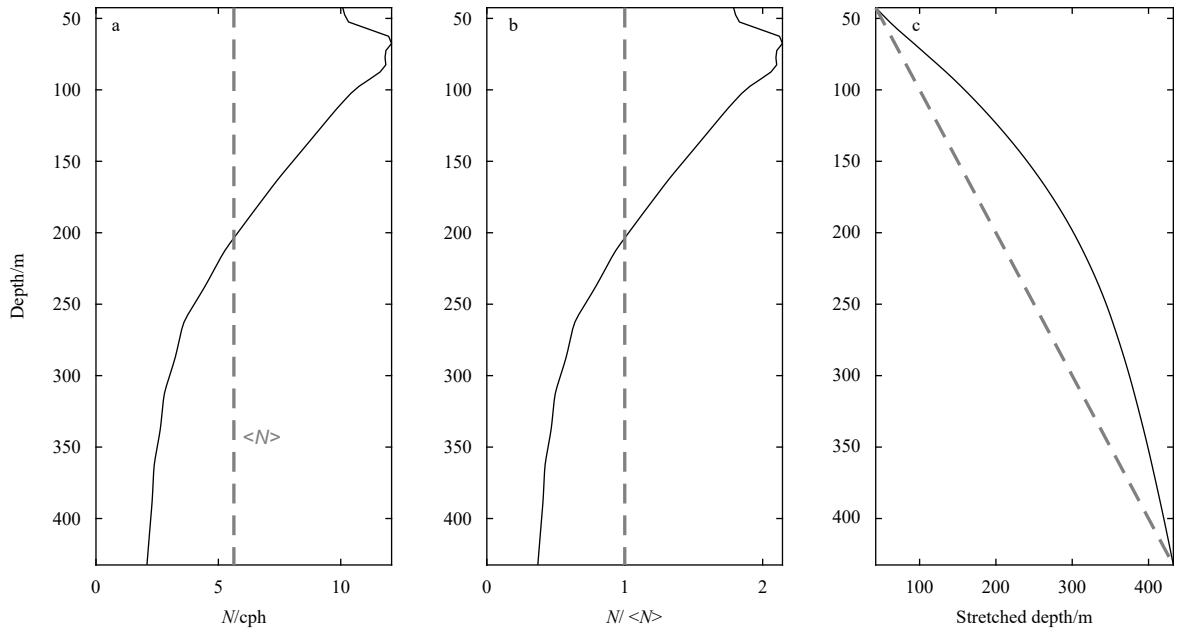

Fig. 3. Buoyancy frequency profile and the WKB-stretched depth. The annual-mean profile of buoyancy frequency from WOA2018 (a), WKB-scale factor (b), and the WKB-stretched depth versus actual depth (c).

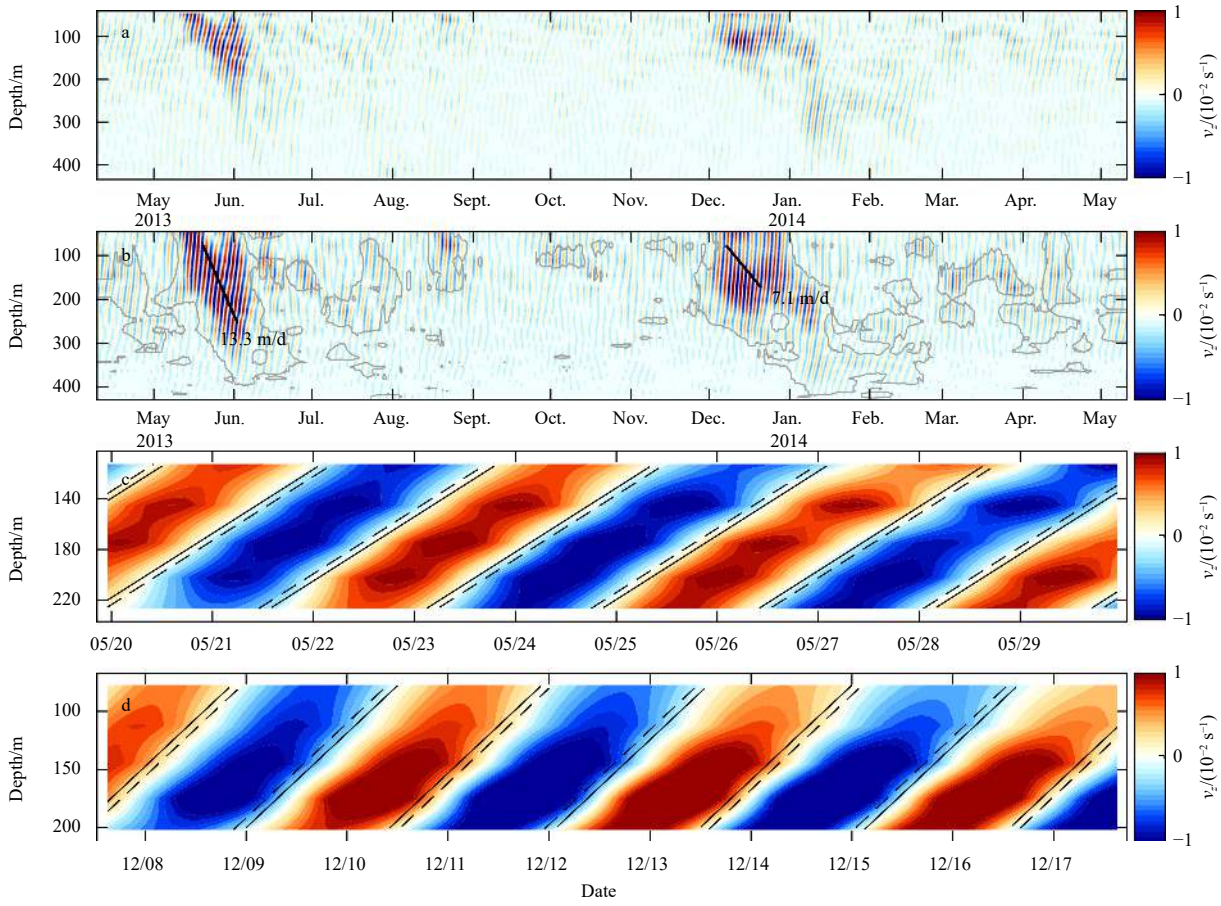

Fig. 4. Near-inertial shear and plane wave solutions. a. Bandpass filtered near-inertial meridional shear from April 9, 2013 to May 11, 2014. b. Same as a, but for the bandpass filtered near-inertial meridional shear with WKB scaling. The gray lines give the areas where vector correlation coefficients between the total shear and the near-inertial shear exceeds 0.7. The black lines indicate the rays of NIWs propagating downward, and the group velocity is shown along the side. c. Snapshot of the TC Viyaru case between 112 m and 227 m (stretched depth). The time ticks are in format mm/dd. d. Same as c, but for the TC Madi case between 77 m and 202 m (stretched depth). The solid and dashed lines represent contours of 0.1 and –0.1 of the plane wave solutions, respectively.

dows, giving the vertical wavenumber-frequency spectrum as follows:

$$\Phi = < \widetilde{w}\widetilde{w}^{*} > /(\Delta\omega\Delta m), \tag{5}$$

where $\Delta\omega$ and Δm are the frequency and vertical wavenumber resolution, respectively. The resulting spectrum divided the variance into four quadrants. Positive/negative frequencies and wavenumbers indicate counterclockwise/clockwise rotation over time and with increasing depth, respectively. Clockwise polarization with depth (negative frequency) indicates downward energy propagation for freely propagating linear internal waves under well-stratified conditions (Leaman and Sanford, 1975; Alford et al., 2012; Gao et al., 2019). The rotary frequency spectrum was given by integrating the 2D spectrum on the vertical wavenumber as follows:

$$\Phi(\omega) = \int_{-m_N}^{m_N} \Phi(\omega, m)\mathrm{d}m, \tag{6}$$

where $m_N = 1/32$ cpm, is the Nyquist wavenumber.

The rotary frequency spectrum above was further divided into two parts, Φ_{cw} for negative frequencies (clockwise) and Φ_{ccw} for positive frequencies (counterclockwise). The criterion that the Φ_{cw}/Φ_{ccw} ratio is larger than 3 was applied to define the near-inertial band for each frequency spectrum, which was also accepted by the following calculations of shear variances in different frequency bands. By integrating the spectrum in negative/positive wavenumbers, the downward (upward)-propagating components were obtained. The contribution of shear variance for a specified frequency band was defined as the sum of the shear variance in that band divided by the total variance as follows:

$$R_{sh} = \sum \Phi_{band} \Big/ \sum \Phi. \tag{7}$$

3 Results

Figure 5 gives the wavenumber-frequency spectra for the different forcing periods marked in Fig. 2. The 2D spectra have two prominent peaks in frequency, which are the near-inertial and the low-frequency (subinertial) peak. The near-inertial peak is nearly clockwise polarized with very little variance found around positive *f*. The strength varies across different forcing periods. Significantly higher peaks are found during TC processes, and the strength is one or two orders higher than other periods, which coincides with the much higher near-inertial energy flux into the mixed layer from TCs. The subinertial peak is secondarily significant and has a lower vertical wavenumber than the near-inertial peak. The observed frequencies are also shown to shift from the local inertial frequency, *f*. Figure 5e shows an obvious shift to the lower frequency near *f*. Doppler shifting caused by the M_2 internal tide can also be found in most periods, whereas the variances of the interferential frequencies ($M_2 + f$ and $M_2 - f$) are much lower than those of the near-inertial peaks.

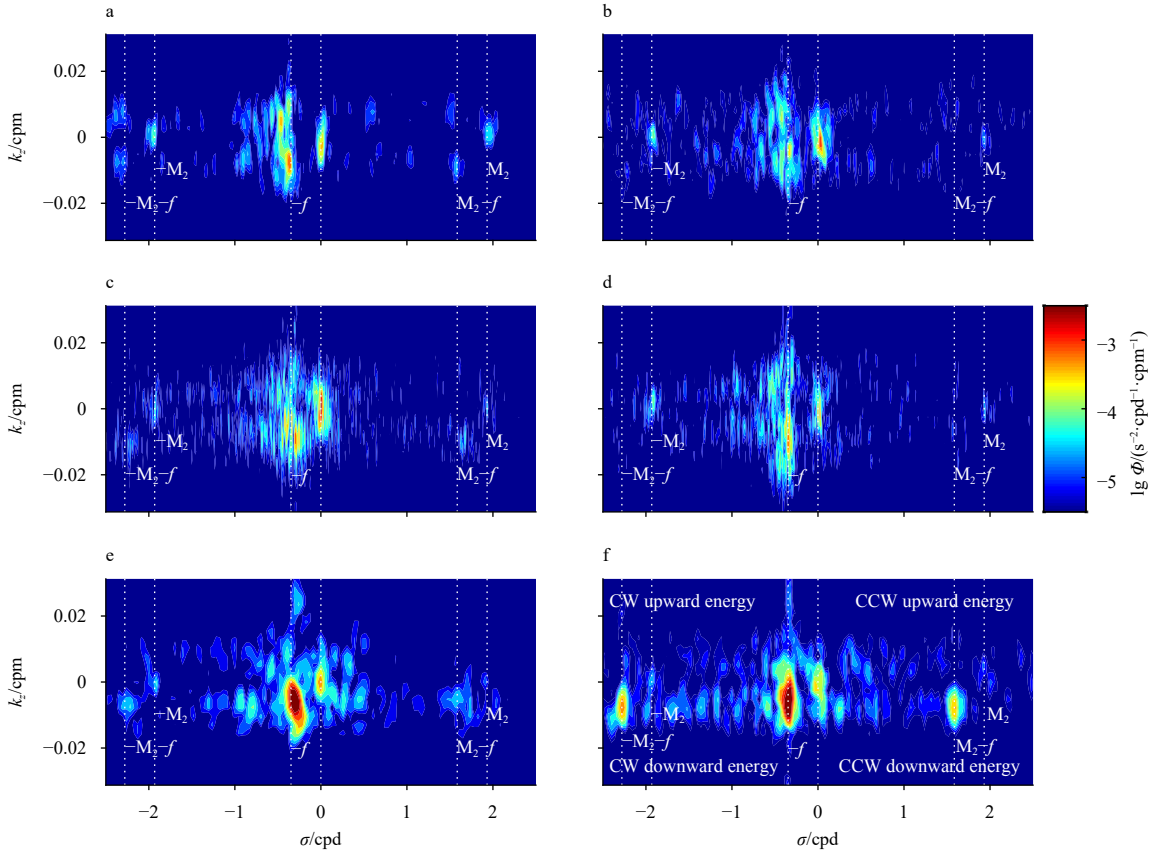

Fig. 5. Wavenumber-frequency spectra for different periods. a. Pre-monsoon, b. post-monsoon, c. summer monsoon, d. winter monsoon, e. TC Viyaru, and f. TC Madi. The division of the periods is the same as that presented in Fig. 2. The gray dashed lines represent different frequencies, and the corresponding frequencies are shown. The abscissa is wave frequency, σ, in cycle per day (cpd), and the ordinate is vertical wavenumber, k_z, in cycle per meter (cpm).

The rotary frequency spectra for the different forcing periods are given in Fig. 6. The near-inertial peaks are evident in all panels and dominated by the downward components. In the continuum higher than f and lower than M_2, the spectra closely follow the Garret and Munk internal wave spectrum GM76 (Garret and Munk, 1975; Cairns and Williams, 1976). The elevated peaks at M_2–f and M_2+f during TC Madi (Fig. 6f) are unexpected since these two peaks are significantly lower in other periods. To illustrate the unusual increases in the interferential peaks, we need more information about tidal displacements in the water column; currently, this data is now only available under 280 m. This topic is discussed in the next section.

The spectra provide an opportunity to examine the shear features for different forcing periods. During the summer monsoon and post-monsoon seasons, the near-inertial peaks are slightly lower than those during the winter monsoon and subsequent pre-monsoon seasons. This can be qualitatively related to fewer NIW events occurring during the summer and post-monsoon seasons, as shown in Fig. 4b. During TC processes, the near-inertial shear variance is one or two orders higher and almost dominated by downward components. The peak frequency during TC Viyaru is approximately 0.304 3 cpd (about 0.88f), which is nearly identical to that given by the plane wave solution. An apparent frequency shift is also found during the summer monsoon, suggesting an effective inertial frequency lowered by background vorticity.

Based on the spectral analysis above, it is straightforward to estimate the shear variances and quantify their proportions in the total in different frequency bands for different periods. The results are given in Table 1. Clearly, the near-inertial shear contributes a large portion of the total and in fact is dominant during the TCs and during winter and pre-monsoon seasons. Moreover, the near-inertial shear is dominated by a downward component regardless of season. The proportions of the near-inertial shear are lower than those of the subinertial shear during summer and post-monsoon seasons, although the difference between them is low. The shear variances contained in the M_2 internal tide are much lower than those in the former two frequency bands, which indicates a relatively low shear contribution associated with the baroclinic tide at the mooring site. The averaged proportion of near-inertial shear variances for the whole 13-month record is approximately 50%, higher than those in the summer and winter monsoon seasons and in the post- and pre-monsoon seasons.

It is more intuitive to view the shear contributions by the histogram with error bars, as presented in Fig. 7. Note that the maximum error appears in summer, which means the relatively large uncertainty in the estimates of shear variance during this period. This, as illustrated in the rotary frequency spectrum (Fig. 6c), could arise from the existence of mesoscale eddies that shed lower frequencies than the near-interial bands (NIB). It is interesting that the proportion of near-inertial shear variance for the whole record is higher than that for any other seasons except for

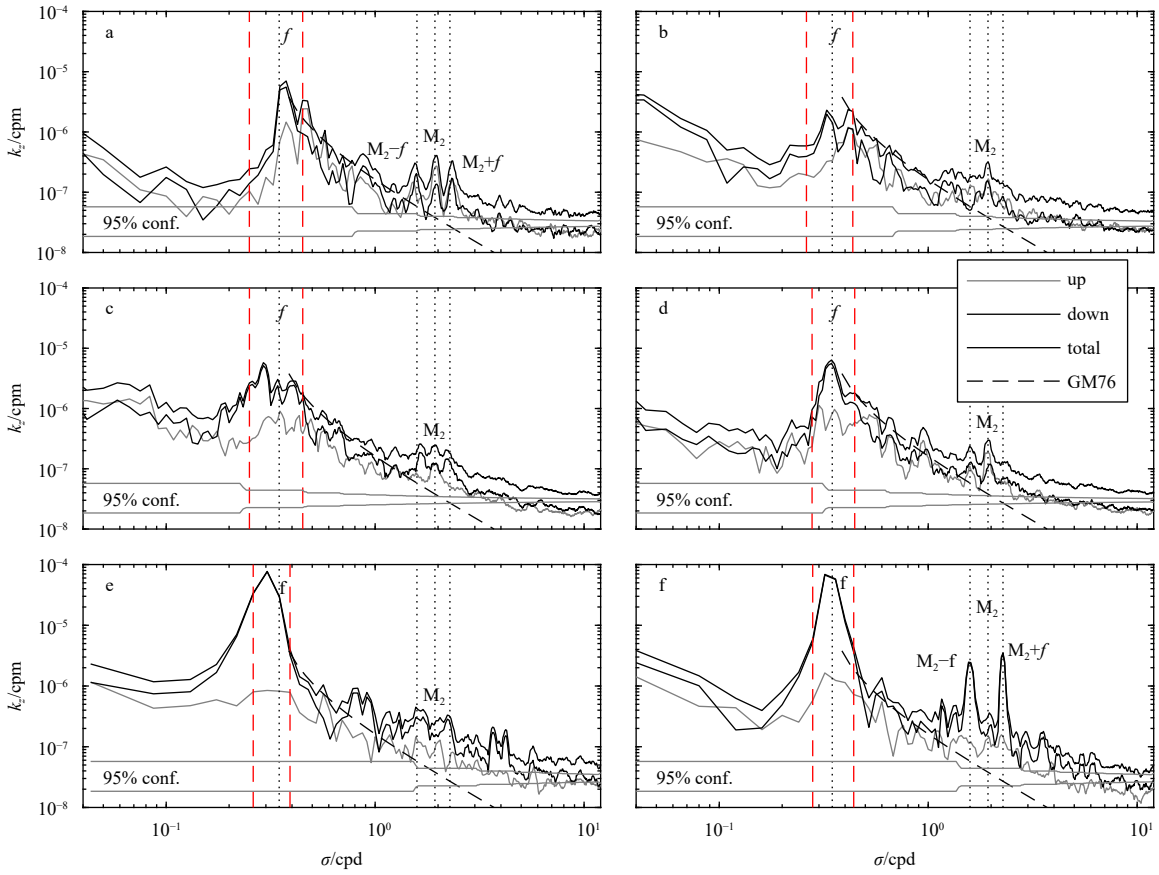

Fig. 6. Rotary frequency spectra for different periods. a. Pre-monsoon, b. post-monsoon, c. summer monsoon, d. winter monsoon, e. TC Viyaru, and f. TC Madi. The red dashed lines indicate the near-inertial frequency bands determined by the ratio of clockwise and counterclockwise components exceeding 3 (see the text). Horizontal gray lines give the confidence intervals of the spectra, with degrees of freedom varying with increasing frequency, σ, in cycle per day (cpd), and the ordinate is vertical wavenumber, k_z, in cycle per meter (cpm).

the TCs, which indicates that the near-inertial shear variance during TCs accounts for a considerable part of the annual mean, though the TCs were short in duration. This is consistent with the near-inertial energy input patterns of 2013 presented in Fig. 1. From the perspective of the annual mean, the near-inertial energy input into the mixed layer is mostly contributed by the short-term TC processes, which is also true for the shear variance.

4 Discussion

4.1 *Subinertial shear by mesoscale eddy*

The above analysis reveals a fact that the proportion of near-inertial shear variance in the total is lower in summer than in winter. This is explained by the rotary frequency spectrum and attributed to the effect of mesoscale eddies during the summer monsoon. With the help of mooring temperature observations and contemporaneous SLA data, it is possible to confirm this. As shown by the mooring temperature in Fig. 8, there was an obvious warm eddy passing through the mooring from late July to mid-September 2013. As seen in the SLA and surface geostrophic current patterns, the warm eddy began to affect the mooring in late July. The eddy center passed through the mooring in late Au-

Table 1. Percentage of shear variances in the total variances

Period	NIB	SubIB	M_2
Pre-monsoon	44.5 (32.5)	9.0	5.9 (2.6)
Post-monsoon	27.2 (17.8)	30.3	6.3 (3.8)
Summer monsoon	33.9 (27.6)	35.6	3.6 (2.4)
Winter monsoon	42.6 (34.1)	14.8	4.9 (2.7)
TC Viyaru	80.2 (78.5)	7.7	1.1 (0.9)
TC Madi	74.8 (72.2)	4.3	1.2 (0.90)
Whole record	49.5 (44.5)	20.3	3.4 (2.2)

Note: The columns give the estimates for near-inertial bands (NIB), subinertial bands (SubIB) and M_2 internal tide bands. The values in the parentheses give the percentage of the downward-propagating shear in the total shear.

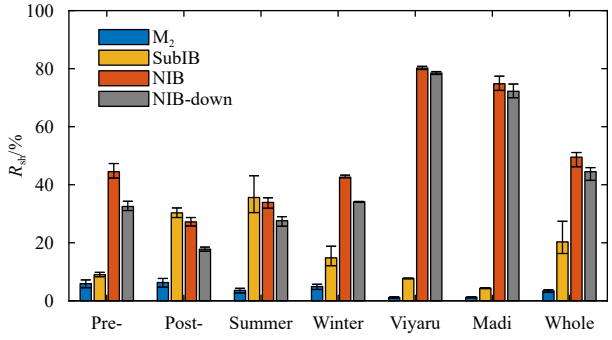

Fig. 7. Histogram of the percentage of shear variances in total variances. The error bars were estimated by the corresponding 95% confidence intervals given in Fig. 6.

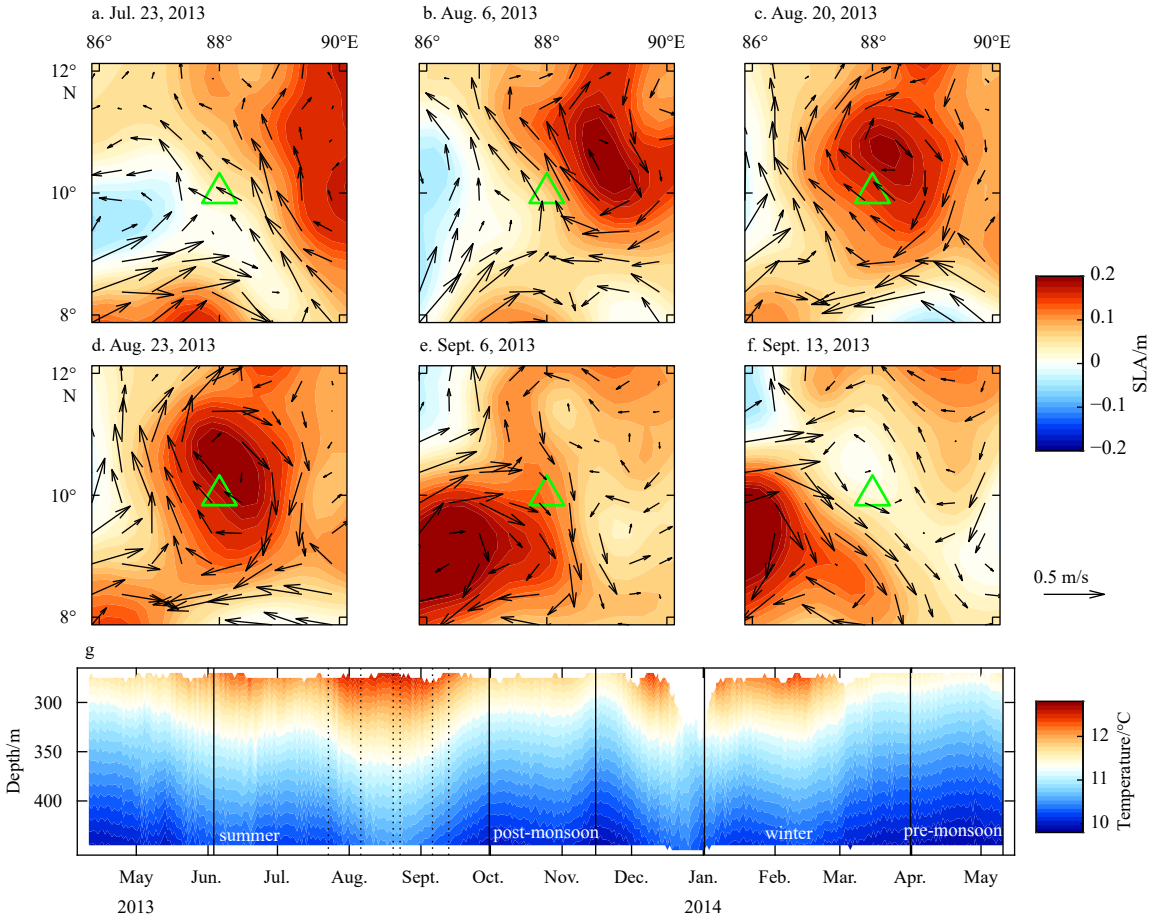

Fig. 8. Sea surface anomaly (SLA; a–f) and mooring temperature observations (g) . SLA and surface geostrophic currents correspond to the dates indicated by the dashed lines in g. The green triangle represents the location of the mooring. Contours of temperature data are beneath 280 m in g. The black solid lines in g give four of the six periods indicated by the red dashed lines in Fig. 2.

gust, and the eddy moved away in mid-September. The whole process lasted for nearly 50 d and induced significant fluctuations in the isopycnal as well as subinertial current shear. In contrast, the upper ocean during the winter monsoon seemed more quiescent, and thus, the subinertial shear variance was lower.

4.2 *Doppler shift by internal tide*

The shear was computed by differencing the velocity in the fixed range bins, while the shear layers can be vertically shifted by the internal tides. This gives rise to the vertical Doppler shift effect that has been discussed previously by Pinkel (2008). The Doppler shift can be partly eliminated by introducing a semi-Lagrange coordinate in which the vertical coordinate follows the isopycnal displacements induced by the internal tides (Alford et al., 2017). In our analysis, due to the lack of temperature observations shallower than 280 m, it is not possible to directly project the shear onto the semi-Lagrange frame. The shear data were thus computed under the Eulerian frame, which may lead to biases in shear variance estimates in the near-inertial bands. However, owing to the relatively low contribution of shear variances in the M_2 internal tide bands as well as the interferential frequency bands, this effect would not result in considerable error in the estimates in Table 1, in which the near-inertial and subinertial shear are basically much higher than that contaminates.

The Doppler shift from the internal tide caused the apparent $M_2 + f$ and M_2–f peaks in the rotary frequency spectrum, e.g., that during TC Madi in Fig. 6f. The two peaks occurred with distinct appearances during the different forcing periods (Fig. 6), which can be directed to the synchronicity between the NIW events and tidal phases. When the NIW events interact with the strong tide periods, e.g., spring tide, the shear layers can be largely displaced and appear as interferential peaks between inertial and tidal motions.

An example is presented in Fig. 9. Here, a backrotation method was applied to examine the shear with rotation sense removed (Alford et al., 2017). This was done by multiplying the shear data by a backrotation operator $e^{i\omega t}$, where ω is the observed near-inertial frequency that can be derived from the frequency spectrum or the plane wave solution. Superimposed on the backrotated shear contours are the internal tide displacements derived from the semidiurnal tidal component of the isotherm of 11°C (at a mean depth of approximately 350 m). The internal tide displacements beyond the observation depths were reconstructed through a dynamic modal analysis method (Figs S2 and S3). During TC Viyaru and Madi, the near-inertial peaks are similar in strength, while the interferential peaks are quite different (Figs 6e and f). The backrotated shear layers were evidently displaced both up and down in tidal frequency (Figs 9b and d). When compared with the internal tide displacements, the NIW events following TC Madi appeared along with the spring tide cycle (Fig. 9c), whereas the other case following TC Viyaru occurred with the neap tide cycle (Fig. 9a). After a few days, about a week, the tidal phases switched while the internal tide displacements in the case of Madi (neap tide) were still comparable with that in the case of Viyaru (spring tide), and the fluctuations in the shear layers were still apparent. Therefore, the shear variances

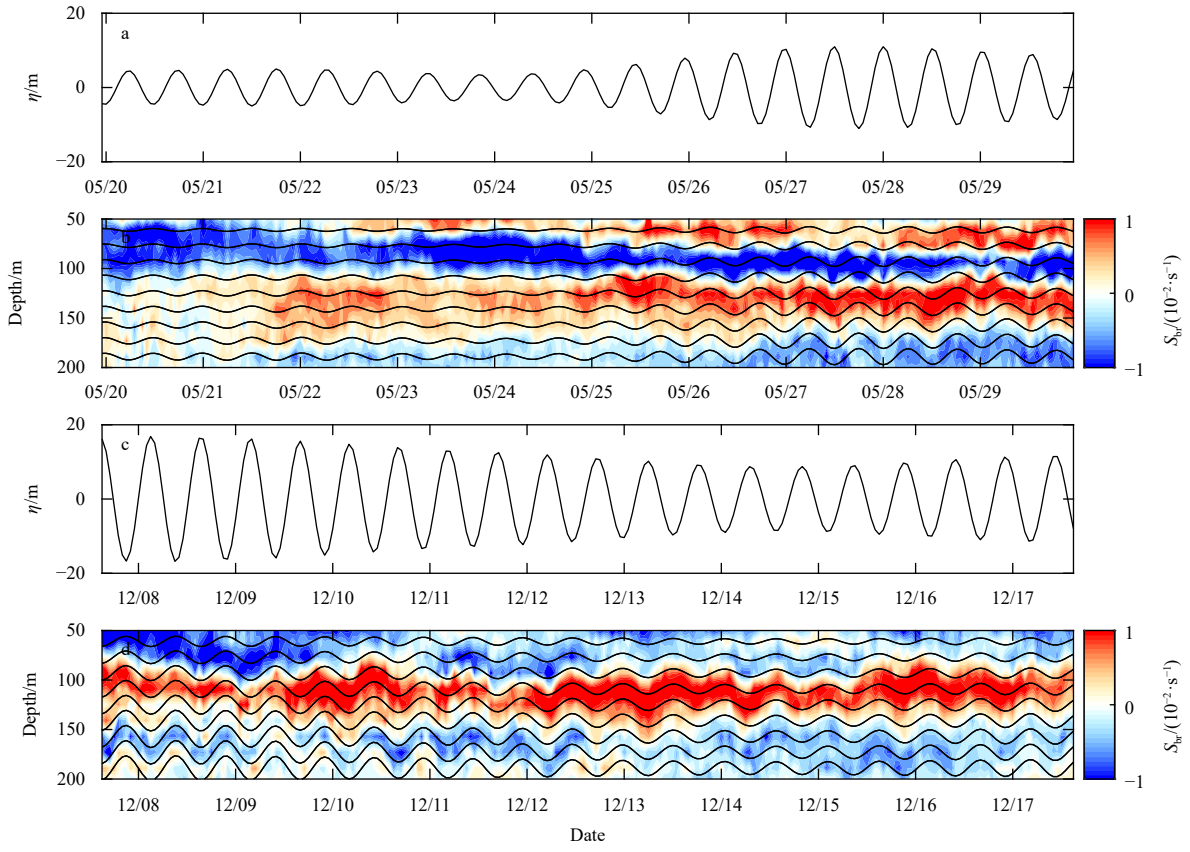

Fig. 9. Backrotated shear and internal tide displacements. M_2 tidal components of the isotherm of 11°C for TC Viyaru (May 2013) (a) and TC Madi (December 2013) (b). The corresponding real part of the backrotated shear (S_{br}) between 50 m and 200 m with internal tide displacements superimposed (black solid lines) (b, d).

near the interferential frequencies are more apparent during TC Madi.

4.3 *Mixing effect of NIWs*

A recent study suggested that in weak and constant trade wind-dominated regions, TCs are a significant factor in the supply of energy that is available for diapycnal mixing (Köhler et al., 2018). Since the persistence time of TC forcing is much shorter than that of monsoonal winds, its effect on the variability of large-scale processes is seemingly underestimated, although it inputs far higher near-inertial energy from the atmosphere to the upper ocean than those under constant wind conditions, such as monsoons (Fig. 1). Moreover, the TC-related NIWs can propagate downward into deeper regions, and the associated high shear layers can last for 20–30 d at the low latitudes of the BoB, where the local inertial period is nearly 3 d. Such an influence of TC-related NIWs may not be well represented by those models using forcing from inaccurate TC winds. Previous work by Rimac et al. (2013) found a strong sensitivity of near-inertial energy input to wind forcing, which points to a possible underestimation of the wind-generated energy available for deep ocean mixing in previous studies based on low-resolution winds.

As revealed by Jochum et al. (2013), the parameterization of NIWs can deepen the surface mixed layer up to 30%, leading to a change in sea surface temperature and precipitation in tropical oceans. For the BoB, the analysis showed that shear by NIWs is dominant in the total shear or at least comparable to the shear by subinertial motions in the monsoon seasons when TC is not active. However, related research is not available on how the occupation of such a large portion of shear by the NIWs can affect the vertical mixing of the upper ocean and further contribute to the heat and salt budget in the BoB, and this topic warrants further study.

5 Summary and conclusions

Shear features were examined using the velocity profiles acquired from a 13-month subsurface mooring observation in the BoB. It was achieved mainly by applying a two-dimensional Fourier transform on the WKB-scaled shear data. The data allow us to estimate the proportion of shear in the total in different frequency bands for different monsoon seasons and for different TC processes by examining the rotary frequency spectra. The shear by NIWs is shown to contribute nearly 50% to the total in the upper layers of the BoB for the whole record. The high proportion is mainly due to the enhancement of the TC processes during which the near-inertial shear accounts for nearly 80% of the total. The seasonality of the near-inertial shear variance was also analyzed. The proportion of near-inertial shear is lower during the summer monsoon than during the winter monsoon owing to more active mesoscale eddies and higher subinertial shear during the summer monsoon. The M_2 internal tide introduced interferential peaks between the inertial and tidal frequencies but has little effect on the main results since the proportion of shear induced by tidal motions is much lower than that by near-inertial and subinertial motions.

Since the annual-mean near-inertial energy flux in the BoB is mostly determined by the TC processes and the annual-mean near-inertial shear is elevated due to the enhancement of the TCs, it is proposed that NIWs following TCs would have a critical effect on the upper ocean heat and salt budget if correctly parameterized in the coupled models. Moreover, it is shown that in the steady wind periods such as the summer and winter monsoons, the near-inertial shear is dominant in the total or at least comparable with the subinertial shear, which underscores the need for further study on the performances of models with the parameterization for NIWs incorporated.

Acknowledgements

We thank the captain and crews of the R/V *Shiyan* 3 for helping us to deploy and recover the mooring. The NCEP CFSv2 wind data are acquired from https://rda.ucar.edu/datasets/ds094.0/. The WOA2018 temperature and salinity data are download from https://www.nodc.noaa.gov/OC5/woa18/, and the daily SLA data are acquired from the SSALTO/Duacs products distributed by AVISO+ (https://www.aviso.altimetry.fr/). The observation data used to construct the figures and tables in this work are available and provided by the corresponding author.

References

Alford M H. 2003. Improved global maps and 54-year history of wind-work on ocean inertial motions. Geophysical Research Letters, 30: 1424

Alford M H, Cronin M F, Klymak J M. 2012. Annual cycle and depth penetration of wind-generated near-inertial internal waves at Ocean Station Papa in the northeast Pacific. Journal of Physical Oceanography, 42: 889–909, doi: 10.1175/JPO-D-11-092.1

Alford M H, Gregg M C. 2001. Near-inertial mixing: Modulation of shear, strain and microstructure at low latitude. Journal of Geophysical Research: Oceans, 106: 16947–16968, doi: 10.1029/2000JC000370

Alford M H, MacKinnon J A, Pinkel R, et al. 2017. Space-time scales of shear in the North Pacific. Journal of Physical Oceanography, 47: 2455–2478, doi: 10.1175/JPO-D-17-0087.1

Alford M H, MacKinnon J A, Simmons H L, et al. 2016. Near-inertial internal gravity waves in the ocean. Annual Review of Marine Science, 8: 95–123, doi: 10.1146/annurev-marine-010814-015746

Breaker L C, Gemmill W H, Dewitt P W, et al. 2003. A curious relationship between the winds and currents at the western entrance of the Santa Barbara Channel. Journal of Geophysical Research, 108: 3132, doi: 10.1029/2002JC001458

Cairns J L, Williams G O. 1976. Internal wave observations from a midwater float. Journal of Geophysical Research, 81: 1943–1950, doi: 10.1029/JC081i012p01943

Cao Anzhou, Guo Zheng, Wang Shuya, et al. 2019. Upper ocean shear in the northern South China Sea. Journal of Oceanography, 75: 525–539, doi: 10.1007/s10872-019-00520-x

Cherian D, Shroyer E, Wijesekera H, et al. 2020. The seasonal cycle of upper-ocean mixing at 8°N in the Bay of Bengal. Journal of Physical Oceanography, 50: 323–342, doi: 10.1175/JPO-D-19-0114.1

Chowdary J S, Parekh A, Ojha S, et al. 2016. Impact of upper ocean processes and air-sea fluxes on seasonal SST biases over the tropical Indian Ocean in the NCEP Climate Forecasting System. International Journal of Climatology, 36: 188–207, doi: 10.1002/joc.4336

Garrett C. 2001. What is the "near-inertial" band and why is it different from the rest of the internal wave spectrum?. Journal of Physical Oceanography, 31: 962–971, doi: 10.1175/1520-0485(2001)031<0962:WITNIB>2.0.CO;2

Garrett C, Munk W. 1975. Space-time scales of internal waves: A progress report. Journal of Geophysical Research, 80: 291–297, doi: 10.1029/JC080i003p00291

Gao Jing, Wang Jianing, Wang Fan. 2019. Response of near-Inertial shear to wind stress curl and sea level. Scientific Reports, 9: 1–11

Girishkumar M, Suprit K, Chiranjivi J, et al. 2014. Observed oceanic response to tropical cyclone Jal from a moored buoy in the south-western Bay of Bengal. Ocean Dynamics, 64: 325–335, doi: 10.1007/s10236-014-0689-6

Goswami B, Rao S A, Sengupta D, et al. 2016. Monsoons to mixing in the Bay of Bengal: Multiscale air-sea interactions and monsoon

predictability. Oceanography, 29: 18–27
Jochum M, Briegleb B P, Danabasoglu G, et al. 2013. The impact of oceanic near-inertial waves on climate. Journal of Climate, 26: 2833–2844, doi: 10.1175/JCLI-D-12-00181.1
Johnston T S, Chaudhuri D, Mathur M, et al. 2016. Decay mechanisms of near-inertial mixed layer oscillations in the Bay of Bengal. Oceanography, 29: 180–191, doi: 10.5670/oceanog.2016.50
Köhler J, Völker G S, Walter M. 2018. Response of the internal wave field to remote wind forcing by tropical cyclones. Journal of Physical Oceanography, 48: 317–328, doi: 10.1175/JPO-D-17-0112.1
Leaman K D, Sanford T B. 1975. Vertical energy propagation of inertial waves: A vector spectral analysis of velocity profiles. Journal of Geophysical Research, 80: 1975–1978, doi: 10.1029/JC080i015p01975
Majumder S, Tandon A, Rudnick D L, et al. 2015. Near inertial kinetic energy budget of the mixed layer and shear evolution in the transition layer in the Arabian Sea during the monsoons. Journal of Geophysical Research: Oceans, 120: 6492–6507, doi: 10.1002/2014JC010198
Pinkel R. 2008. Advection, phase distortion, and the frequency spectrum of finescale fields in the sea. Journal of Physical Oceanography, 38: 291–313, doi: 10.1175/2007JPO3559.1
Rimac A, von Storch J S, Eden C, et al. 2013. The influence of high-resolution wind stress field on the power input to near-inertial motions in the ocean. Geophysical Research Letters, 40: 4882–4886, doi: 10.1002/grl.50929
Saha S, Coauthors. 2014. The NCEP Climate Forecast System Version 2. Journal of Climate, 27: 2185–2208, doi: 10.1175/JCLI-D-12-00823.1
Schott F A, Xie S P, McCreary J P. 2009. Indian Ocean circulation and climate variability. Reviews of Geophysics, 47: RG1002
Varkey M J, Murty V S, Suryanarayana A. 1996. Physical oceanography of the Bay of Bengal and Andaman Sea. Oceanography and Marine Biology, 34: 1–70

Supplementary information:

Fig. S1. Annual-mean near-inertial energy flux to the mixed layer in the Bay of Bengal.

Fig. S2. Buoyancy frequency profile and the modal function. a. Buoyancy frequency profile computed from WOA2018 climatological temperature and salinity data. b. The modal function of the first mode computed using buoyancy profiles in the left panel. The red solid line in each panel gives the profile used in the calculations for the internal tide displacements, and the red dashed line in the right panel indicates the averaged depth of 11°C at about 350 m.

Fig. S3. M2 internal tide displacements (solid lines) extracted from the mooring temperature observation (color). The two cases presented are the same as those shown in Fig. 9: TC Viyaru (a) and TC Madi (b). The isotherms selected in both panels are ranging from 10.5°C to 12°C with an interval of 0.25°C. The reconstructed displacements are computed relative to the isotherm of 11°C near 350 m by multiplying the displacement at each intended depth by the coefficient given by the red solid line in the right panel of Fig. S2.

The supplementary information is available online at https://10.1007/s13131-021-1743-0 and www.aosocean.com. The supplementary information is published as submitted, without typesetting or editing. The responsibility for scientific accuracy and content remains entirely with the authors.